Implementation of Finite Rate Chemistry Capability in OVERFLOW

M. E. Olsen [*]
NASA Ames Research Center
Moffett Field, CA 94035
S. Venkateswaran [†]
University of Tennesse
Tullahoma, TN, 37388
D. K. Prabhu [‡]
ELORET Corp.
Sunnyvale , CA 94087

An implementation of both finite rate and equilibrium chemistry have been completed for the OVERFLOW code, a chimera capable, complex geometry flow code widely used to predict transonic flowfields. The implementation builds on the computational efficiency and geometric generality of the solver.

Nomenclature

$\bar{\gamma}$	$\rho c^2/p$
ϵ	internal energy($\int_0^T c_v dT$)
η	Self Similar Wall Distance for Wedge ($(z - z_w)/x$)
ν_{rs}^b	Backward Stoichiometric Coefficient of species s in reaction r
ν_{rs}^f	Forward Stoichiometric Coefficient of species s in reaction r
∂_n	Spatial derivative in wall normal direction
ρ	total mass per unit volume($\sum_s^{n_s} \rho_s$)
ρ_s	mass of species s per unit volume
ξ	Dimensionless Axial Distance for Wedge(x/L)
c	Frozen Sound Speed, $\partial_\rho p\big|_{s,y_i}$
c_s	Mass fraction of species s, ρ_s/ρ
h_T	stagnation enthalpy ($(e_i + p/rho + (u^2 + v^2 + w^2)/2)$
L	Wedge Length(x/L)

Introduction

Chemically reacting flows are of increasing importance to NASA's terrestrial and space missions. In cases where the flow geometry is complex, which includes most practical devices, ability to utilize overset grids greatly enhances NASA's ability to accurately model the flow physics. The OVERFLOW code is therefore an ideal platform for implementing chemical modeling capability. This provides the ability to

predict performance and improve design of both reentry vehicles and propulsion systems. In this paper we discuss the approach for incorporating finite rate chemistry capability into OVERFLOW and present representative computations along with comparisons with experiment.

Method

The base code used is OVERFLOW[1] which is a finite difference, chimera(overset) grid capable, complex geometry flow code widely used for perfect gas prediction. Various ADI implicit treatments (Beam-Warming, Pulliam-Chausee diagonal, Symmetric LU Gauss Seidell) are available, along with a selection of spacial discretization options (central differnce with scalar or matrix dissipation, Roe MUSCL upwinding, Yee's Symmetric TVD, etc.). Multigrid convergence acceleration is available, and improves the convergence of high Reynolds number viscous flows substantially. The dual time scheme implemented in the perfect gas version of OVERFLOW allows time accurate calculations to be free of factorization and chimera interface 'lag'.

Matrix dissipation combined with central space differencing and multigrid was shown to provide a rapid, robust solution method suitable for high speed, perfect gas flow with strong shock waves.[2] The first step in the generalization of the gas model of overflow was to implement the premixed chemical equilibrium gas model of Liu and Vinokur.[3] Preliminary experiments with this implementation verified that the central/matrix dissipation methodology continued to work with more general thermodynamics.[4]

OVERFLOW was modified to replace the perfect gas model built into the code with a model assum-

[*]Research Scientist, NASA Ames Research Center, Associate Fellow AIAA
[†]Research Professor, University of Tennessee, Member AIAA
[‡]Senior Research Scientist, ELORET, Associate Fellow AIAA

ing a gas made up of a mixture of thermally perfect ($p_i = \rho \mathcal{R} T / \mathcal{M}_i$) gases. This modification affects a large fraction of the code, which used perfect gas assumptions to obtain pressure and temperature from the conservative field variables. Four extra field variables are added, corresponding to pressure, temperature, Prandtl number, and gas constant.

Chemically Reacting Reynolds Averaged Navier Stokes Equations

The Reynolds averaged Navier-Stokes equations, written in conservation law form are

$$\frac{\partial Q}{\partial t} + \frac{\partial F}{\partial x} + \frac{\partial G}{\partial y} + \frac{\partial H}{\partial z} = 0 \qquad (1)$$

Where

$$Q = [\rho, \rho u, \rho v, \rho w, \rho \epsilon,] \qquad (2)$$

$$F = \left[\rho u, \rho u^2 + p + \tau_{xx}, \rho u v + \tau_{xy}, \rho u w + \tau_{xz} \right.$$
$$\left. \rho u (\epsilon_T + p + \tau_{xx}) + v \tau_{xy} + w \tau_{xz} + k \frac{\partial T}{\partial x} \right] \qquad (3)$$

$$G = \left[\rho v, \rho v u + \tau_{yx}, \rho v^2 + p + \tau_{yy}, \rho v w + \tau_{yz}, \right.$$
$$\left. \rho v (\epsilon_T + p + \tau_{yy}) + w \tau_{yz} + u \tau_{yx} + k \frac{\partial T}{\partial y} \right] \qquad (4)$$

$$H = \left[\rho u, \rho w u + \tau_{zx}, \rho w v + \tau_{zy}, \rho w^2 + p + \tau_{zz}, \right.$$
$$\left. \rho w (\epsilon_T + p + \tau_{zz}) + u \tau_{zx} + v \tau_{zy} + k \frac{\partial T}{\partial z} \right] \qquad (5)$$

The Navier-Stokes equations for a chemically reacting gas are similar to this set, except that the 1st equation (mass conservation) is replaced by n_s equations, one for each chemical species.

$$\partial_t \rho_i + \partial_x \left(u \rho_i + (D \partial_x \rho_i) \right) + \partial_y \left(v \rho_i + (D \partial_y \rho_i) \right)$$
$$+ \partial_z \left(w \rho_i + (D \partial_z \rho_i) \right) = \dot{w}_i \quad (6)$$

These equations add a mass diffusion term $(\partial_\xi D (\partial_\xi \rho_i))$ and a source term $\dot{w}_i$. The standard form for the source terms is

$$\dot{w}_i = \mathcal{M}_i \sum_r^{n_r} \left(\nu_{ri}^b - \nu_{ri}^f \right) k_r^f A_r \qquad (7)$$

$$A_r = \prod_s^{n_s} \left[\frac{\rho_s}{\mathcal{M}_s} \right]^{\nu_{rs}^f} - \left[\frac{p}{p_{ref}} \right]^{-\Delta \nu_r} \frac{1}{K_r^e} \prod_s^{n_s} \left[\frac{\rho_s}{\mathcal{M}_s} \right]^{\nu_{rs}^b} \qquad (8)$$

where the r sums the contributions of the individual reactions, k^f is the forward reaction rate and K_r^e is the equilibrium constant (a pure function of temperature), p_{ref} is the pressure reference for K^e, and $\Delta \nu_r = \sum_s^{n_s} \nu_{rs}^f - \sum_s^{n_s} \nu_{rs}^b$.

In this form, the significance of K_e is obvious. In the case where the mass fractions satisfy the relation

$$\left(\frac{p}{p_{ref}} \right)^{\Delta \nu_r} K_r^e \prod_s^{ns} \left(\frac{\rho_s}{\mathcal{M}_s} \right)^{\nu_{rs}^f} = \prod_s^{ns} \left(\frac{\rho_s}{\mathcal{M}_s} \right)^{\nu_{rs}^b} \qquad (9)$$

for reaction r, the source term for this particular reaction will be zero. K^e can be calculated from equilibrium thermodynamics, or can be specified independently. Both options are available in the current implementation.

In the current implementation, the original Navier-Stokes equations(1-5) are solved, with the species fractions held constant, The species equations (6) are then solved holding the velocities and temperatures from the mean flow equations just calculated. This over specifies the problem, as the mass conservation equation is contained in the species mass conservation equations. Although various methods of removing this over-specification were attempted, the current method simply ignores the over-specification, and utilizes the ρ_i to get the partial pressures, and ρ as the total mass density. As the solution converges, the ratio $\sum_i^{n_s} \rho_i / \rho$ is used to verify convergence along with the equation residual levels.

Generalization of the Thermodynamic Model

At the start of each step, just before the viscosity is calculated, the temperature is found for each point from the current internal energy and species concentrations, via a Newton-Raphson iteration. This temperature can then be used to find the pressure at each point, by summing the partial pressures of each gas ($p = \sum_{species} p_{species}$). The Prandtl number is calculated from Euken's relation.[5] The gas constant is calculated from the species fractions and their molecular weights.

The internal energy and absolute entropy of each species as a function of temperature are input as a table to generalize the thermodynamic model. The table has the following format:

N_T	T_0	ΔT	
$\mathcal{NAME}_1$			
$\mathcal{M}_1$	ΔH_{f1}		
T_0	$\hat{e}_0 / \mathcal{R} T$	$\hat{s}_0 / \mathcal{R}$	
T_1	$\hat{e}_1 / \mathcal{R} T$	$\hat{s}_1 / \mathcal{R}$	
....			
T_{N_T}	$\hat{e}_{N_T} / \mathcal{R} T$	$\hat{s}_{N_T} / \mathcal{R}$	
$\mathcal{NAME}_2$			
$\mathcal{M}_2$	ΔH_{f2}		
T_0	$\hat{e}_0 / \mathcal{R} T$	$\hat{s}_0 / \mathcal{R}$	
T_1	$\hat{e}_1 / \mathcal{R} T$	$\hat{s}_1 / \mathcal{R}$	
....			
T_{N_T}	$\hat{e}_{N_T} / \mathcal{R} T$	$\hat{s}_{N_T} / \mathcal{R}$	
$\vdots$			
$\mathcal{NAME}_{N_s}$			
$\mathcal{M}_{N_s}$	ΔH_{fN_s}		
T_0	$\hat{e}_0 / \mathcal{R} T$	$\hat{s}_0 / \mathcal{R}$	
T_1	$\hat{e}_1 / \mathcal{R} T$	$\hat{s}_1 / \mathcal{R}$	
....			
T_{N_T}	$\hat{e}_{N_T} / \mathcal{R} T$	$\hat{s}_{N_T} / \mathcal{R}$	

where species 1, species 2, ... species N_t label the blocks.

The first line gives the number of (equis-

paced) temperature values used(N_T), the starting temperature($T_0(K°)$), and the temperature spacing ($\Delta T(K°)$). The second line is chemical formula for the species, such as H2O for water, O2 for diatomic oxygen, etc. The next line is the molecular weight in kg/kmole and the heat of formation in KJoules/kg. The next N_T lines are the values of $T(K°)$, internal energy(non dimensionalized by $\mathcal{R}(T)$), and entropy(non-dimensionalized by $\mathcal{R}$). This is then followed by a similar set of lines for the each species in turn. The order of the species in this file is the order of the species stored in the solution file, and the order of species for specifying reactions rates, etc.

This choice of functional form for the table, and hence the cubic spline fits also results in a smaller variation over in the functional values (at least for ϵ) over large temperature ranges. A species with constant specific heat would have the $\epsilon/\mathcal{R}T$ column a constant. Tables have been created for 5 species air ($[N_2, O_2, NO, N, O]$, from[3]), and hydrogen-air ($[H_2, N_2, O_2, HO, H, O, H_2O, HO_2, H_2O_2]$, from NIST polynomial fits).

Polynomial fits, such as the Lewis, or NIST curve fits may be input by creating a table by evaluating the polynomials and writing out the values of T, $\hat{e}/(\hat{\mathcal{R}}T$ and $\hat{s}/\hat{\mathcal{R}}$. Energy and absolute entropy are both input, so that chemical equilibrium or finite rate chemistry may be calculated. This also allows the backward rate for the chemistry to be calculated from the forward rate and the 2nd law of thermodynamics.

The field equations for convection of species are also available in the perfect gas version of OVERFLOW. These were replaced with a generalized upwind or central convection, 2nd order mass diffusion, and generalized chemical source module. These are currently solved uncoupled from the fluid and turbulence field equations. A fast source calculation procedure was implemented, so that the source flux and Jacobian requires about the same amount of computational effort as the efficient Pulliam-Chausee diagonal fluids step.

Chemical Reaction Specification

The chemical reactions are input in the OVER-FLOW input file, in a new namelist section in the input file $CHEM. The number of reactions NRE-ACT, the number of elements NELEM, the distribution of elements amount the various species scoef(ispecies,jelem), the stoichiometric coeficients vnuf(ireact,ispecies), vnub(ireact,ispecies, and the reaction forward and backward rates fcoef(:,ireact), ecoef(:,ireact) are all specified in this section. William Chan has written a version of the overgrid[6] which facilitates the input of these variables. This software, reads the thermodynamics input files gas.tbl described above, and parses out the scoef matrix from the species names, and then allows reactions to be specified in an intutive manner. The system also checks for ele-ment balance among the chemical reactions input, and requires the reactions to balance elements between forward and backward sides.

A decision was made to consistently use SI units when dimensional values were necessary, such as for T_∞, p_∞, reaction rates, etc. The units used then are kmoles, m, kg, $K°$ and sec. A great deal of the chemical reaction data is in cgs (moles, cm, g, and sec) units and factor of 10^{-3} will transform a reaction rate from $cm^3/(mole\ sec)$ to $m^3/(kmole\ sec)$. The forward rate is input in the Arrenhius form $k_f = C_1(T)^{C_2}exp(C_3/T)$, and the backward rate is determined either from an equilibrium coefficient $k_e = k_b/k_f = k_e(ecoef_i, T)$ in the modified Arenhius form used in reference,[7] or directly from the 2nd law of thermodynamics.

The reactions are specified separately, so each that third body reactions is input separately. This greatly expands the size of this input section, but allows for complete generality in fixing the forward and backward rate of each reaction for the various third bodies. The chemical source calculation procedure goes through the complete reaction set, and groups reactions from the same third body reaction together, taking account of the variations in the forward and backward rates among the group of various third body species, for computational efficiency.

For the species equations, both central and 2nd order upwind are available, and solutions using both approaches are given in the results section. There are cases for which the upwind method is more robust, but once initial transients are eliminated, the central space version is more robust (can run at higher CFL) and accurate (as shown by the element conservation).

Transport Properties

The diffusion operator for the species equations is 2nd order accurate, and the binary diffusion coefficients and laminar viscosities are given by Leonard-Jones theory, with a Wilke mixing rule. Euken's relation is used to give the molecular thermal conductivity, or Prandtl number, of the gas mixture. Turbulence is modelled by any of the available turbulence models in OVERFLOW. The effect of turbulence is only to increase the effective viscosity, binary diffusivity, and heat transfer. No enhancement of the reaction rates is currently modelled.

Computational Efficiency

A finite rate simulation is a little more than 3 times as expensive per iteration as a corresponding simulation using the perfect gas version of OVERFLOW. The additional work (with a perfect gas simulation as a unit of computational work), is as follows:

Arbitrary Thermodynamics(single species)	0.25
Species Convection, etc.(5 species)	1.5
Source Flux/Jacobian (5 species)	0.5

Note that the species convection/diffusion includes the pre-multiplication by a 5×5 matrix, required for the ADI solution of the species equations with implicit source terms. This is substantial work compared to the ADI inversion itself, and makes the species field operator an expensive part of this good breakfast, er, flow solver.

Non-Premixed Chemical Equilibrium Capability

Along with the new finite rate capability, an ability to accurately simulate flows in chemical equilibrium has been implemented. This capability was envisioned as a means of providing a robust starting solution capability for difficult flowfields. This capability does not require that the flow be premixed, so that equilibrium diffusion flame calculations are possible. For flowfields where chemical equilibrium is a valid assumption, this provides a robust and more simply specified simulation capability.

This capability is provided by a similarity transformation of the species variables. The species can be thought of as composed of linear combinations of the elements. For instance, water (H_2O) can be thought of as 2 parts hydrogen to one part oxygen (on a molar basis). A linear combination of the species then can be used to compute the molar concentraion of each element, given the species concentrations. For a chemical system composed of n_e elements, and n_s species, there are n_e linear equations which will give the amount of each element given the species concentraions. Furthermore, on physical grounds, these n_e equations are independent, and thus define a n_e dimensional subspace within the n_s dimensional species space. A method equivalent to Gram-Schmidt orthogonalization can then generate the remaining $n_s - n_e$ linear relations which will transform the original species variables into a new combinations where n_e of the new variables correspond with the elements, and the remaining $n_s - n_e$ variables correspond to the degrees of reaction freedom of the system.

This transformation can (and has been) automated, and has some desirable properties which merit exploration. One of these properties is that by transforming the species equations to this new independent variable set separates out the n_e zero eigenvalues of the source jacobian matrix. More than this, these variables have zero source, so they could be separated from the other $n_s - n_e$ variables, and solved as simple convection diffusion equations. The other 'reaction freedom' variables can then be solved as the original species set, with non-zero sources, and a matrix block size reduced by the n_e elements sepatated out at considerable compuational savings.

Currently, this "element splitting" is utilized to im-

plement the non-premixed chemical equilibrium capability of the code. The species are split, and the equations for the element conservation are solved. The 'reaction freedom' variables are solved for by enforcing chemical equilibrium at each point.

Multigrid, Relaxation, and Chemistry-Fluid Coupling

The multigrid method[8] has been modified to enhance the robustness of the method. The original multigrid method used a linear interpolation of the conservative variables to map the coarse grid solution onto the next finer grid. This interpolation was replaced with a linear interpolation of the variables $[\rho, u, v, w, \epsilon]$, which ensures a positive value of ϵ on the finer grid if ϵ is positive on the coarser grid. With this modification, the multigrid method continues to be a net win, enhancing robustness and improving convergence rates.

The Pulliam–Chaussee diagonal algorithm is used for the mass, momentum and energy equations, and enhances the computational efficiency. This implicit operator requires that the eigensystem (here essentially just the sound speed) be modelled correctly. The frozen sound speed $\left.\frac{\partial p}{\partial \rho}\right|_{s,c_i}$, is calculated by $(\bar{\gamma}p/\rho)$, with $\bar{\gamma} = 1 + \frac{R}{C_v}$.

The chemistry implementation is currently a loosely coupled approach, with the changes in mass, momentum and energy variables $\{\rho, \rho u, \rho v, \rho w, \rho \epsilon\}$ solved for holding species concentration fixed, and then changes in species concentration $\{c_i\}$ are determined by solving the conservative form of the species transport equations holding the conservative variables constant.

Boundary Conditions

A new boundary condition was implemented for chemically reacting flowfields, the catalytic fixed temperature wall. The non-catalytic boundary condition for the species is zero gradient in species fractions. A catalytic wall boundary condition is given as

$$\mathcal{D}\partial_n(\rho_{N_2}) = \rho_N \gamma_c \left(\frac{\mathcal{R}T}{2\pi \mathcal{M}_N}\right)^{\frac{1}{2}}$$

$$\mathcal{D}\partial_n(\rho_N) = -\rho_N \gamma_c \left(\frac{\mathcal{R}T}{2\pi \mathcal{M}_N}\right)^{\frac{1}{2}}$$

$$\mathcal{D}\partial_n(\rho_{O_2}) = \rho_O \gamma_c \left(\frac{\mathcal{R}T}{2\pi \mathcal{M}_O}\right)^{\frac{1}{2}}$$

$$\mathcal{D}\partial_n(\rho_O) = -\rho_O \gamma_c \left(\frac{\mathcal{R}T}{2\pi \mathcal{M}_O}\right)^{\frac{1}{2}}$$

$$\mathcal{D}\partial_n(\rho_{NO}) = 0 \tag{10}$$

where the value of γ_c is 0 for a non-catalytic wall, or 1 for a fully catalytic wall.

This is implemented in a general way by defining

the diffusion potential of the species j as

$$W_j = \rho_j \left(\frac{\mathcal{R}T}{2\pi\mathcal{M}_j} \right)^{\frac{1}{2}}$$

then we can write a general version of this boundary condition as

$$\mathcal{D}\partial_n(\rho_j) = \sum_k C_{jk} W_k \tag{11}$$
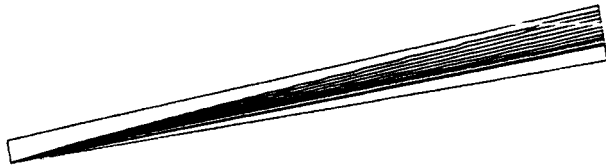
where C_{jk} is a $n_s \times n_s$ matrix.

Results

Fig. 1 10°M=25 Inviscid Wedge Grid, Colored by Axial Velocity

Inviscid Wedge Flow

This flowfield is a self similar flowfield useful for gauging the ability to capture shocks at oblique angles to the grid, and to obtain the external inviscid flowfield downstream of the shock. The case considered here is a 10° wedge, at M=25.083, with freestream static conditions of $p_\infty = 100$KPa, $T_\infty = 2000°$K. The species for this case are $\{N_2, O_2, NO, N, O\}$. The thermodynamic data for these species ($cv(T)$) are from the calculations outlined in Liu.[3]

A converged solution is shown in Figure 1. The capture of the oblique shock is clearly demonstrated, with uniform conditions obtained on both sides of the shock. The shock crosses the grid system obliquely, with the shock moving out one grid line for every two gridlines moved downstream.
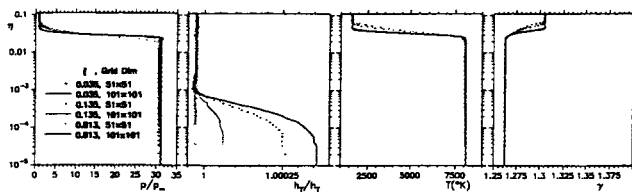
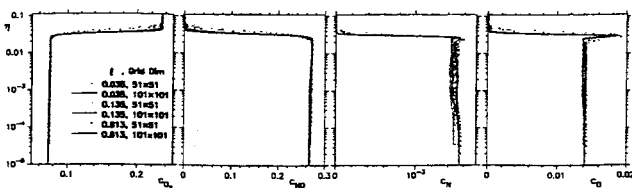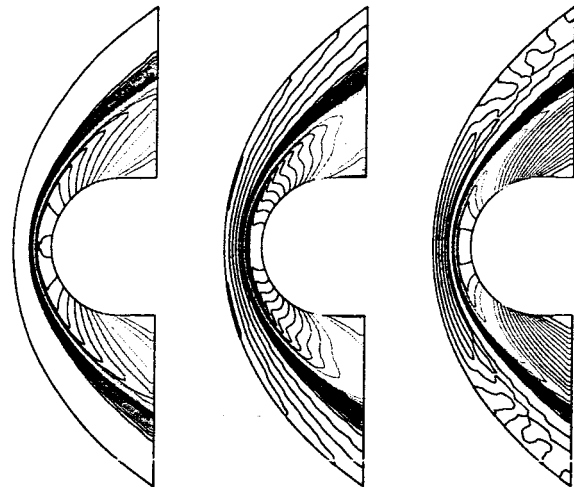**Fig. 2** Inviscid M=25 Wedge, Profiles of Pressure, Total Enthalpy, Temperature and γ

Fig. 3 Inviscid M=25 Wedge, Mass Fraction Profiles

| a) Pressure | b) Temperature | c) Density |

Fig. 6 Circular Cylinder Flowfield: $M_\infty = 12.7$, $r = 1$m, $h = 40$km, $|v| = 4.04$km/s

Profiles of pressure, total enthalpy, temperature, and pressure are shown in Figure 2. The pressure profile shows minimal overshoot, with good similarity between the various axial locations The total enthalpy is well conserved (for this flowfield it is constant), with errors, even at the shock, less than 0.5%. Total enthalpy errors behind the shock are less than 0.1%. The post shock temperature reached in this flowfield is 8000°K, for which there is appreciable dissociation, as shown by the gamma variation from 1.32(freestream) to 1.26(post shock).

The species mass fractions are shown in Figure 3. Almost all the diatomic oxygen (O_2) is dissociated across the shock, and is transformed into nitrous oxide (NO). Elemental oxygen (O) and nitrogen (N) are at low levels post shock.

The forward and backward rate for this calculation are given by Parks model,[7] and in the full paper this will be compared with solutions using backward rates derived from the forward rates and the equilibrium constants given by the 2nd law.

2D Cylinder Flow

As a comparison to other Codes, a solution for a 1m radius circular cylinder at 40km altitude, $u_\infty = 6$ km/sec (figure) is compared with solutions from GASP. The flow conditions for this case are $M_\infty = 12.7$, $Re_r = 9690$, $T_\infty = 251.05°$K, and $p_\infty = 277.5$Pa. The freestream mass fractions are $c_{N_2} = 0.767$, $c_{O_2} = 0.233$ with traces of NO, N, and O. Two wall boundary conditions are evaluated, non catalytic and catalytic fixed temperature, with $T_w = 2553°$K.

The dimensions of the finest grid were 101×101, and the solution was evaluted on coarser grids of 51×51 and 26×26 to assess grid convergence. The coarser grids were obtained from the finer grid by successively deleting every other point. Wall normal spacing for the
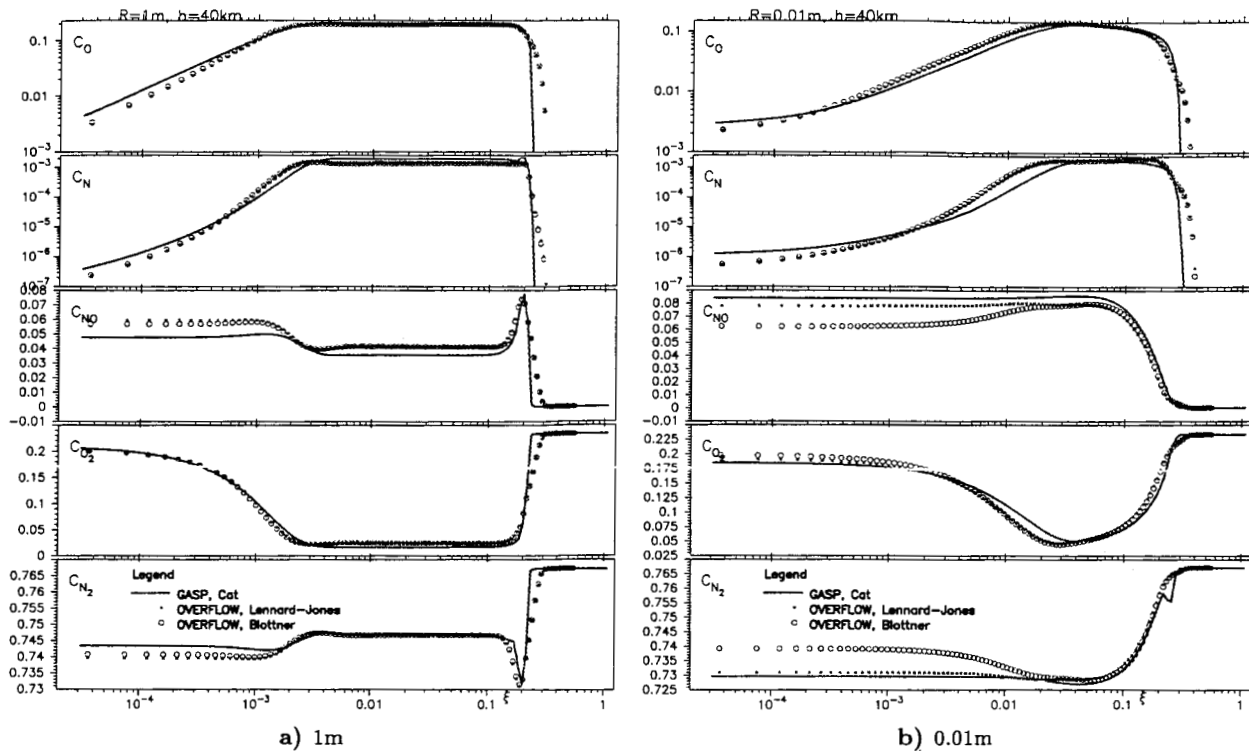
Fig. 4 2D Cylinder Stagnation Line Mass Concentrations, $M_\infty = 12.7$, $r = 1m$, $h = 40km$, $|v| = 4.04km/s$

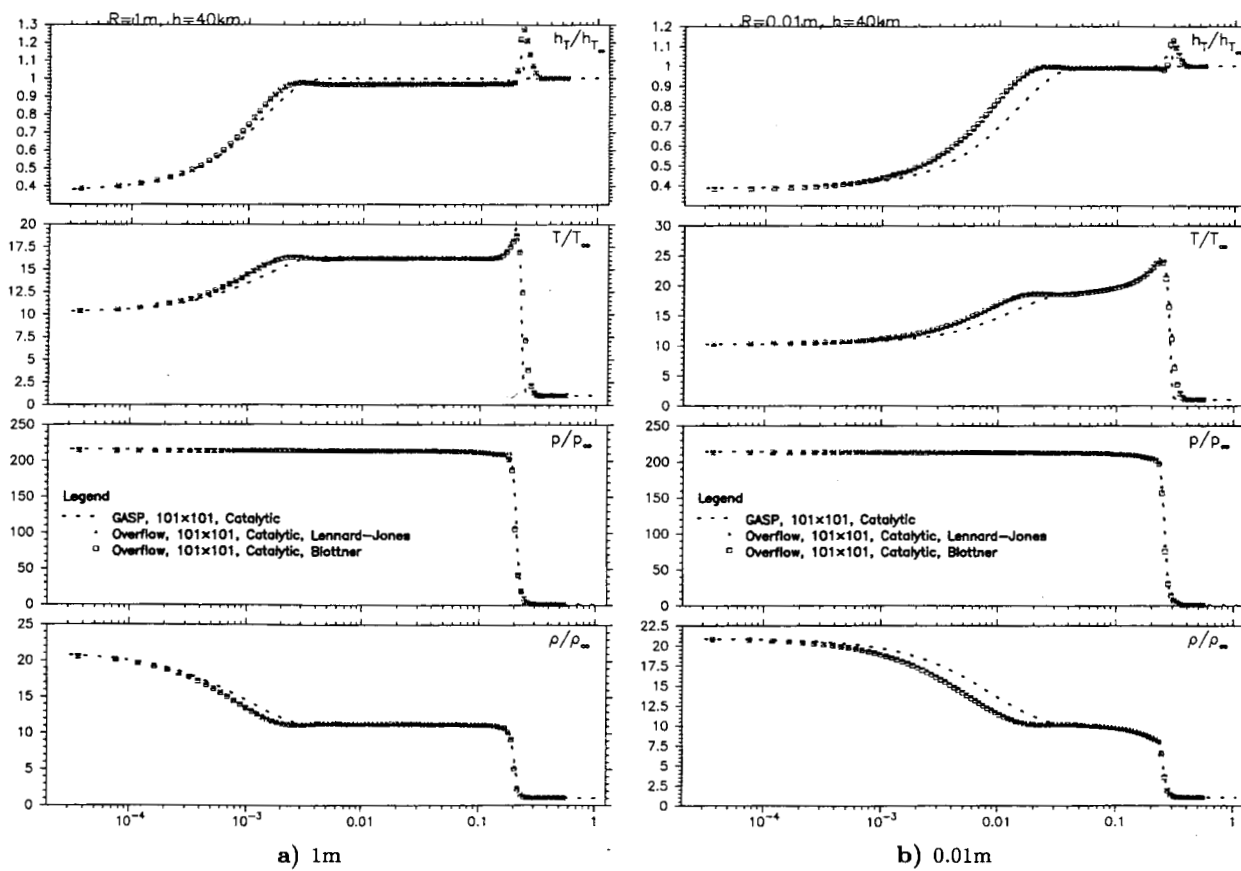**Fig. 5 2D Cylinder Stagnation Line Thermodynamic State, $M_\infty = 12.7$, $r = 1m$, $h = 40km$, $|v| = 4.04km/s$**

AMERICAN INSTITUTE OF AERONAUTICS AND ASTRONAUTICS PAPER 2004-XXXX

finest grids was 3×10^{-5} for both GASP and OVER-FLOW.

One reaction model for this case was created by using the forward rates of the Park model, and backward rates from equilibrium thermodynamics. A second model uses Park's equilibrium coeffiecient curve fits for $\bar{n} = 1e18$, as $K^e(T)$, then setting $p_{ref} = 100Pa$. These solutions are compared with the solution from GASP, using its coded Park model.

Profiles of the thermodynamic variables along the stagnation streamline are shown in figure 5. Total enthalpy is well conserved across the shock, and the predictions of GASP and the two reaction models are in good agreement. Pressure density are also in very good agreement, and the OVERFLOW solution appears to be grid resolved on the 51×51 grid. Temperature however, is not in as good agreement as the other variables.

The reason for this can be seen from figure 4, where the stagnation line species concentrations are shown. The levels of monatomic nitrogen and oxygen are well predicted, but there is a slight disagreement predictions for NO, N_2, and O_2. These can be traced to differences in the K^e representations, as the results can be brought into much closer agreement by altering the reference pressure for K^e. As there is some slop in the various estimates of K_e for these reactions, this agreement is probably as good as can be expected.
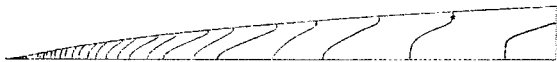
F4 Nozzle Flow

Fig. 7 T10-97 Pressure Predictions, Finite Rate

Another important test case for chemically reacting flows are nozzle flowfields. Test 10-97(figure7) of the HHSFD database is the flow in the ONERA F4 wind tunnel nozzle. This flowfield utilizes synthetic air, containing only nitrogen and oxygen (no argon, CO_2, etc.), with mass fractions of 7/9 and 2/9 respectively. The stagnation chamber of the flowfield has extremely high enthalpy(100 times standard sea level conditions) and extremely high pressure(37.3 MPa), The flow then expands out a axisymmetric nozzle to near vacuum conditions (p=52Pa). The flowfield has been computed with a variety of codes,[9] providing a useful comparison with other codes, as well as experimental data.

Inlet conditions are highly dissociated subsonic flow. Plug flow in chemical equilibrium was imposed at the inlet face of the flowfield, and p_t and T_t were chosen to produce the correct enthalpy and pressure in the stagnation chamber. The Spalart-Almaras turbulence model was used, and the initial ν_T was set to 0.1 laminar viscosity. Tunnel walls are modelled as constant temperature no-slip boundaries, and the exit plane boundary condition is simple extrapolation.

The flow is close to being in chemical equilibrium, and equilibrium codes are as successful as finite rate codes in predicting the nozzle wall pressures. Figure 8 shows a comparison of the wall pressure predictions of the code with experimental values. Also shown are the wall pressure predictions of the code in equilibrium mode (using the Parks equil. coefficients), and the premixed chemical equilibrium version of OVER-FLOW.[4]

Exit pressures are reasonably well predicted for this case, as shown in figure 9, and are very much in
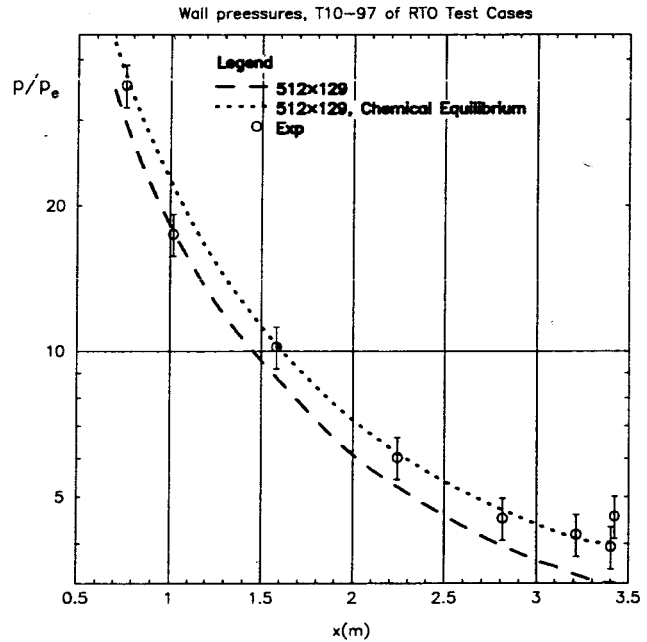

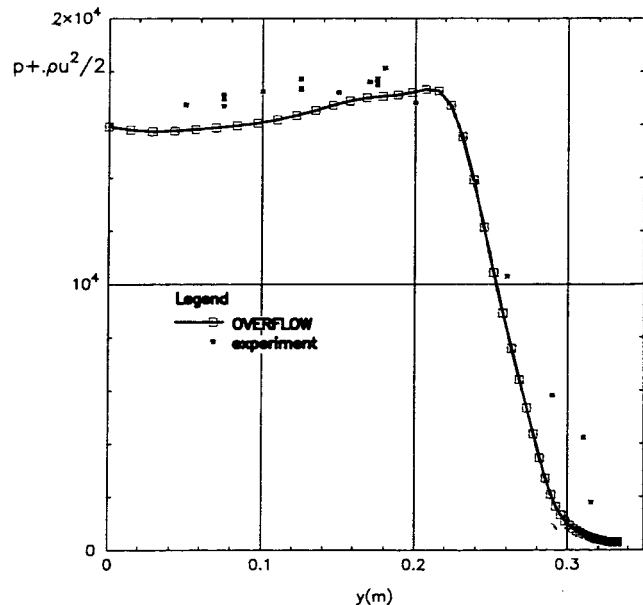**Fig. 8 Wall Pressure Field Predictions, Comparison with Experiment**

Fig. 9 Exit Plane Pitot Pressure Field Predictions, Comparison with Experiment

AMERICAN INSTITUTE OF AERONAUTICS AND ASTRONAUTICS PAPER 2004-XXXX

line with predictions of other nonequilibrium codes for this case. The exit temperature is also well in line with other predictions, and agrees well within the experimental uncertainty (figure 10). A final check is provided by the NO mass fraction prediction, as seen in figure 11. This prediction agrees well with other predictions for this quantity, in terms of the the exit level, and how quickly it approaches this value.

Other Results

Viscous wall solutions for other geometries including 2D and 3D reentry configurations and nozzles, will be presented in the full paper, along with comparison with experimental results.
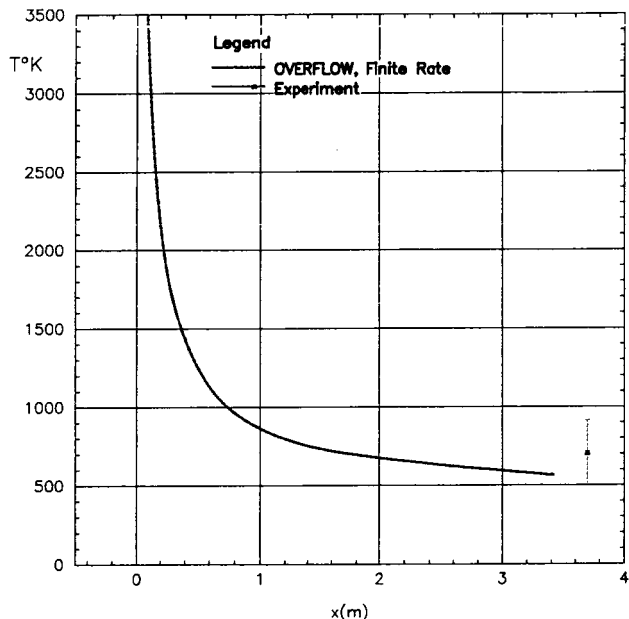

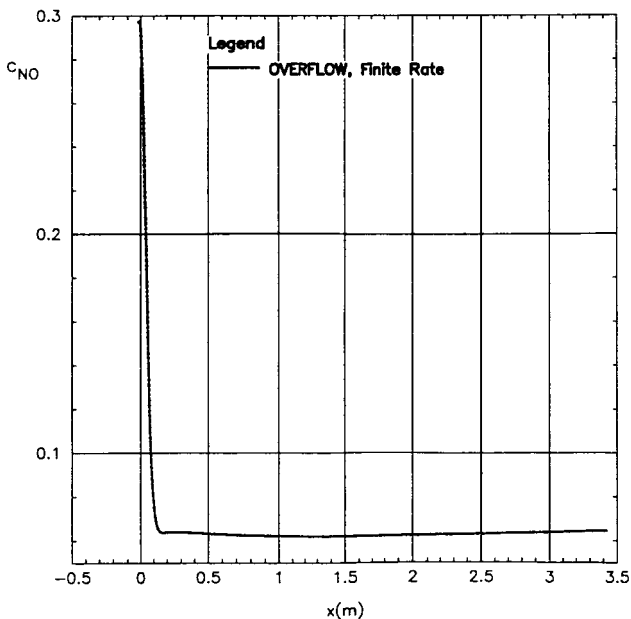**Fig. 10 Centerline Temperature Predictions**

Fig. 11 Centerline NO Mass Fraction Predictions

Conclusions

Finite rate and equilibrium chemistry capability has been added to a version of the OVERFLOW code. The implementation is capable of predicting both combustion and reentry flowfields, and extends the overset capability of OVERFLOW into reacting flowfields.

References

[1] Buning, Pieter G. et al. Overflow user's manual. Version 1.8, NASA Ames Research Center, February 1998.

[2] Olsen, Michael E. and Dinesh K. Prabhu. "Application of OVERFLOW to Hypersonic Perfect Gas Flowfields". AIAA Paper 2001-2664, 2001.

[3] Liu, Yen and Vinokur, Marcel. "Equilibrium Gas Flow Computations. I. Accurate and Efficient Calculation of Equilibrium Gas Properties". AIAA Paper 89-1736, 1989.

[4] Olsen, M. , Liu, Y., Vinokur, M., and Olsen, T. " Implementation of Premixed Equilibrium Chemistry Capability in OVERFLOW". AIAA Paper 2003-0962, 2003.

[5] Rosner, Daniel E. . *"Transport Processes in Chemically Reacting Flow Systems"*. Dover Publications, 2000.

[6] Chan, William M. "The OVERGRID Interface for Computational Simulations on Overset Grids". AIAA Paper 2002–3188, June 2002.

[7] Park, Chul . *"Nonequlibrium Hypersonic Aerothermodynamics"*. John Wiley and Sons, 1990.

[8] Jespersen, D, Pulliam, T. H., and P.G. Buning. Recent enhancements to overflow. AIAA Paper 97-0664, January 1997.

[9] Sagnier, P. and Muylaert, M. "Synthesis of the Contributions to the Test Case T10-97 Wind Tunnel Nozzle". First Europe-US High Speed Flow Database Workshop-Part 2, November 12–14 2000, Naples, Italy, 1997.